

A flexible framework for structural plasticity in GPU-accelerated sparse spiking neural networks

James C. Knight¹, Johanna Senk^{1,2,*} and Thomas Nowotny¹

¹Sussex AI, School of Engineering and Informatics, University of Sussex, Brighton, United Kingdom

²Institute for Advanced Simulation (IAS-6), Jülich Research Centre, Jülich, Germany

*Author to whom any correspondence should be addressed.

E-mail: j.senk@sussex.ac.uk

Keywords: spiking neural network, structural plasticity, topographic map, learning rules

Abstract

The majority of research in both training Artificial Neural Networks (ANNs) and modeling learning in biological brains focuses on synaptic plasticity, where learning equates to changing the strength of existing connections. However, in biological brains, structural plasticity – where new connections are created and others removed – is also vital, not only for effective learning but also for recovery from damage and optimal resource usage. Inspired by structural plasticity, pruning is often used in machine learning to remove weak connections from trained models to reduce the computational requirements of inference. However, the machine learning frameworks typically used for backpropagation-based training of both ANNs and Spiking Neural Networks (SNNs) are optimized for dense connectivity, meaning that pruning does not help reduce the training costs of ever-larger models. The GeNN simulator already supports efficient GPU-accelerated simulation of sparse SNNs for computational neuroscience and machine learning. Here, we present a new flexible framework for implementing GPU-accelerated structural plasticity rules and demonstrate this first using the e-prop supervised learning rule and DEEP R to train efficient, sparse SNN classifiers and then, in an unsupervised learning context, to learn topographic maps. Compared to baseline dense models, our sparse classifiers reduce training time by up to 10× while the DEEP R rewiring enables them to perform as well as the original models. We demonstrate topographic map formation in faster-than-realtime simulations, provide insights into the connectivity evolution, and measure simulation speed versus network size. The proposed framework will enable further research into achieving and maintaining sparsity in network structure and neural communication, as well as exploring the computational benefits of sparsity in a range of neuromorphic applications.

1 Introduction

A simulation of a Spiking Neural Network (SNN) is usually a two-step process: First, data structures for neurons and synapses are instantiated on the machine to define the network, including its connectivity; afterwards, the network state is calculated over time starting from some initial conditions according to the neuron and synapse dynamics. This approach assumes that both neurons and their connectivity are fixed once the network is constructed (typically using population-level connection rules [1]) and at most the strength of connections may be subject to change during the simulation [2]. However, biological evidence suggests that the connectivity itself is continuously changing, not only during development but also in the adult brain [3]. These changes are associated with learning, adaptation, memory, recovery from lesions, drug addiction, and occur following enriched experience, after sensory deprivation or upon stimulation. The generation of new neurons in adult brains (neurogenesis) is less ubiquitous, but has also been observed experimentally – in particular in the rodent hippocampal dentate gyrus [4, 5]. Besides the biological evidence, it has been found that algorithms abstracted from structural plasticity can benefit machine-learning (ML) models. Pruning [6] reduces the parameter count of large models while preserving accuracy and, inspired by neurogenesis, constructive neural networks [7, 8] are ‘grown’ as part of the training process. . The type of structural plasticity addressed in this work

does not add or remove neurons (as in most brain regions beyond development) and concentrates on dynamic formation and elimination of synapses.

To shed light on candidate structural plasticity mechanisms and their function for learning and memory, computational models have been developed to study, for example, whether changes are induced by activity, homeostasis, stochasticity, or other factors. Simulator developers have implemented functionality for modifying network connectivity during runtime to simulate these models, e.g. [9, 10, 11, 12, 13, 14, 15]. However, structural plasticity remains underexplored because simulating networks with it is computationally expensive: First, structural changes in biology are slow (hours, days) and therefore need long simulation durations. Second, there are complex inter-dependencies with other biological mechanisms such as synaptic plasticity and some processes may need global instead of only local information, hence limiting implementations. Third, continuously applying changes to the connectivity clashes with the traditional approach of keeping the network structure untouched in computer memory during state propagation which requires to rethink how data structures are handled. Different simulation platforms including neuromorphic systems therefore face different difficulties.

Structural plasticity algorithms have previously largely been implemented in CPU-based SNN simulators [e.g., 9, 16] and neuromorphic systems such as SpiNNaker [17], where the main computational elements are scalar CPU cores [e.g., 11, 12] and thus the standard routines used for modifying connectivity can be employed. Billaudelle et al. [15] presented a structural plasticity implementation for the BrainScaleS-2 [18] Plasticity Processing Unit (PPU) – a Single Instruction Multiple Thread (SIMD) processor that is tightly integrated with the BrainScaleS-2 neuromorphic system. Here, we propose what we believe is the first structural plasticity framework for implementation on general purpose parallel hardware such as GPUs. The framework aims to combine flexibility (i.e., the possibility to freely explore different structural plasticity mechanisms) with efficiency (i.e., fast simulations). We identify the following constraints:

1. Adding and removing connections cannot require the connectivity data structures to be re-allocated.
2. The amount of data that needs to be moved around when adding or removing a connection must be minimal.
3. The connectivity must still be indexed and read efficiently (i.e., via a coalesced memory read on a GPU).

The GeNN simulator [19, 20] was originally developed for Computational Neuroscience research but its longstanding focus on flexibility and its efficient implementation of sparse data structures on GPU accelerators has enabled it to become a powerful tool for many areas of SNN research. We have previously added support for various machine-learning-specific functionalities including parallel batch simulation of models – allowing multiple copies of the model to be run simultaneously in order to maximize GPU occupancy – and user-defined ‘custom update’ operations [21, 22]. Here, we present a new extension to GeNN which allows users to easily define hybrid CPU/GPU structural plasticity algorithms using the same code-generation based approach already used to define neuron models and learning rules as well as initialization algorithms.

Using this framework we demonstrate two applications. Firstly, building on our previous work [22, 23] using the e-prop learning rule [24] to efficiently train recurrent SNN classifiers, we combine the GeNN implementation of e-prop with the DEEP R structural plasticity rule [25] – implemented in our new framework – to train very sparse networks on the N-MNIST [26] and DVS gesture classification tasks [27] with no loss of accuracy while using 90× fewer parameters than comparable recurrent dense SNN models. The time overhead of applying structural plasticity is less than 1% and the sparse models used are an order of magnitude faster to train than their dense counterparts. Secondly, we implement a model of topographic map formation [28] in GeNN, motivated by a recent example on the SpiNNaker platform [11]. The spatially embedded network employs an activity-independent formation rule: new connections are drawn according to a Gaussian dependence on the lateral distance between neurons. However, synapse elimination is activity-dependent: Spike-Timing-Dependent Plasticity (STDP) [2] varies synaptic strengths and weak synapses are more likely to be removed. The interplay of different plasticity mechanisms in the model results in a refinement of receptive fields and an embedding of learnt input structures in the network connectivity. Even though the large part of the simulation time is here spent on connectivity updates, the simulation is still faster than previous implementations [11] and enables network upscaling experiments to test the scaling performance.

2 Methods

2.1 GeNN custom connectivity updates

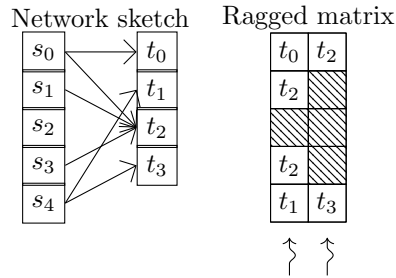


Figure 1. Illustration of data structures used to implement sparse connectivity in GeNN. Five presynaptic neurons are connected to four postsynaptic neurons using sparse connectivity with a maximum out-degree of two. This is represented in memory as a *ragged matrix*, where each row n contains the indices of the target neurons of pre-synaptic neuron n . Spikes are propagated through ragged matrix connectivity by parallelizing across the columns as indicated by the snaking lines.

GeNN [19, 20] is a library for generating CUDA [29] code for the simulation of SNN models. GeNN handles much of the complexity of using CUDA and automatically performs device-specific optimizations so as to maximize performance. GeNN consists of a main library – implementing the API used to define models as well as the generic parts of the code generator – and an additional library for each backend (currently there is a reference C++ backend for generating CPU code and a CUDA backend, with an AMD HIP [30] backend under development). PyGeNN [20] exposes these libraries to Python using PyBind11 [31] and provides a Pythonic and user-friendly interface to the low-level functionality provided by GeNN.

One key advantage of GeNN over SNN simulation libraries such as SNNtorch [32], NORSE [33] or JAXsnn [34] – which are built on standard Machine Learning toolkits like PyTorch or JAX – is that GeNN not only supports standard dense (i.e., all-to-all) weight matrices stored as 2D arrays, but also sparse connectivity stored in the ‘ragged matrix’ data structure illustrated in figure 1. In this data structure, each row contains the indices of a single presynaptic neuron’s postsynaptic targets and, to simplify address calculation, rows are padded to the largest number of postsynaptic targets present in the connectivity matrix. Additional 2D arrays with the same shape are used to store synaptic variables such as weights and delays. To efficiently parallelize the propagation of spikes through this data structure, one CUDA thread is allocated to each column of the matrix. Each thread then loops through incoming spikes, with each ‘warp’ of 32 adjacent threads performing efficient coalesced reads of synaptic weights and accumulating input to the postsynaptic neurons using atomic operations (which on modern GPUs are handled efficiently by the L2 cache). If connectivity updates can be parallelized across presynaptic neurons, this format actually fits the constraints on parallel connectivity updates we defined in the introduction rather well. By adding additional padding to the end of each row, connections can be added and removed without re-allocating the data structure. Because the order of synapses in a row is unimportant, when adding synapses they can simply be added to the end of the row and, when removing them, the synapse at the end of the row can just be moved to the location of the removed synapse and the out-degree reduced by one.

Based on this foundation of efficient, parallel updating of connectivity we reviewed the structural plasticity literature to determine the types of functionality a general structural plasticity framework might need to support.

Access to synaptic weights DEEP R [25] needs to detect changes to the sign of weights and the synaptic rewiring rule developed by Bamford, Murray, and Willshaw [28] compares weights to a threshold.

Additional pre and postsynaptic variables DEEP R [25] needs to track the number of synapses which are removed from each row of the synaptic matrix so they can be summed and the same number of new synapses added.

Access to pre and postsynaptic neuron variables The rule developed by Butz and Ooyen [35] needs to access pre- and postsynaptic calcium variables (essentially low-pass filtered spike trains).

Access to RNG DEEP R [25] needs to be able to sample from a random number generator to create new synapses and the rule developed by Bamford, Murray, and Willshaw [28] uses probabilistic thresholds to determine whether to actually eliminate or add candidate connections.

While, for convenience, GeNN provides some built-in models, one of GeNN’s most powerful features is that it enables users to easily define their own models for neurons, synapses and custom updates (which are typically used to implement optimizers and reductions for machine learning models [23]) from within Python using strings containing GeNNCode which is a subset of C99. Continuing this flexible approach, we have added support for a new model primitive – ‘custom connectivity updates’ – to GeNN which provides a framework to build structural plasticity rules. This framework is relatively complex so, while in the remainder of this section we will try to give a flavor of what is possible, we refer interested readers to the GeNN documentation (<https://genn-team.github.io>) for more details. Rules can be defined with the `pygenn.create_custom_connectivity_update_model` helper function and can access neuron and synapse variables via ‘variable references’ (`pre_var_refs` and `post_var_refs`; and `var_refs` respectively). Additionally, they provide one GeNNCode string which is run on the GPU and parallelized across the *rows* of the synaptic matrix (`row_update_code`) and another that is evaluated serially on the CPU (`host_update_code`). Within all of these code strings, a suitable random number generator is available via a family of `gennrand` functions. Within the `row_update_code`, the index of the presynaptic neuron associated with the row of connectivity can be accessed via the internal variable `id_pre` and synapses can be added using the `add_synapse` function which takes the index the postsynaptic target and the initial values of any synaptic variables, in the order they are specified in `var_refs`. Variables which are associated with the connectivity being updated but are not referenced in this way will be initialized to zero for the new synapse. Using this functionality, we can define a simple example which adds diagonal connections to the connectivity matrix with a synaptic weight (referenced via `g`) of 1.0:

```
1 add_diagonal_model = pygenn.create_custom_connectivity_update_model(
2     "add_diagonal",
3     var_refs=[("g", "scalar")],
4     row_update_code=
5         """
6         add_synapse(id_pre, 1.0);
7         """)
```

An instance of this custom connectivity update could then be attached to an existing synapse group (`sg`) within a model (`model`) and assigned to a ‘custom update group’ called ‘update_connectivity’:

```
1 cu = model.add_custom_connectivity_update(
2     "add_diagonal", "update_connectivity", sg, add_diagonal_model,
3     var_refs={"g": create_wu_var_ref(sg, "g")})
```

At runtime, the update can be triggered (along with any other updates in the ‘update_connectivity’ group) by simply calling `model.custom_update("update_connectivity")`. If row updates need to remove or otherwise access existing synapses they must iterate through them as the rows of the ragged matrix data structure are unsorted. This is implemented by the `for_each_synapse` statement, within the body of which, the index of current postsynaptic targets can be accessed via the `id_post` variable (as well as the values of any variables or variable references associated with individual synapses or postsynaptic neurons). Synapses can also be removed within the body of the `for_each_synapse` statement using the `remove_synapse` function. Finally, custom connectivity updates can define their own additional neuron and synapse variables (`pre_vars` and `post_vars`; and `vars` respectively). Using this additional functionality, we can define another example which, on the CPU, first loops through each presynaptic neuron and picks a random postsynaptic target to try and remove. Then, on the GPU, we search each row of connectivity in parallel and, if the chosen target is found, remove it:

```

1  remove_random_model = pygenn.create_custom_connectivity_update_model(
2      "remove_random",
3      pre_vars=[("postInd", "unsigned int")],
4      row_update_code=
5          """
6          for_each_synapse {
7              if(id_post == postInd) {
8                  remove_synapse();
9                  break;
10             }
11         }
12         """,
13      host_update_code=
14          """
15          for(unsigned int i = 0; i < num_pre; i++) {
16              postInd[i] = genn_rand() % num_post;
17          }
18          pushpostIndToDevice();
19          """

```

In order to facilitate postsynaptic spike-triggered updates to synapses, such as those involved in Spike Timing Dependent Plasticity (STDP), GeNN builds an additional transpose matrix data structure (see [36] for a complete description). This data structure is normally built once at initialization time but, if custom connectivity updates are applied to connections with these data structures, they get rebuilt after each custom connectivity update.

GeNN provides timing functionality – implemented on the GPU using CUDA events and on the CPU using `std::chrono::high_resolution_clock` – to accurately measure the time spent in each simulation kernel and we have extended this same system to enable the timing of the CPU and GPU components of custom connectivity updates as well as of the time spent ‘remapping’ the transpose data structure.

2.1.1 mlGeNN While we have previously implemented complex machine learning workflows with networks of this sort in PyGeNN [22, 21], the syntax is designed for computational neuroscience and it can become tedious and difficult to maintain. Therefore, we have built mlGeNN on top of GeNN to provide a Keras-like abstraction [37, 23] with support for both converting pre-trained ANNs to SNNs and for directly training SNNs using e-prop and Eventprop [38]. Here we have further extended mlGeNN to support DEEP R which can be invoked by creating a sparsely-connected network and ‘compiling’ it using an `EPropCompiler` instantiated as follows:

```

1  compiler = EPropCompiler(
2      example_timesteps=num_timesteps, losses="sparse_categorical_crossentropy",
3      optimiser="adam", batch_size=512,
4      deep_r_conns=[in_hid, hid_hid], deep_r_l1_strength=0.005)

```

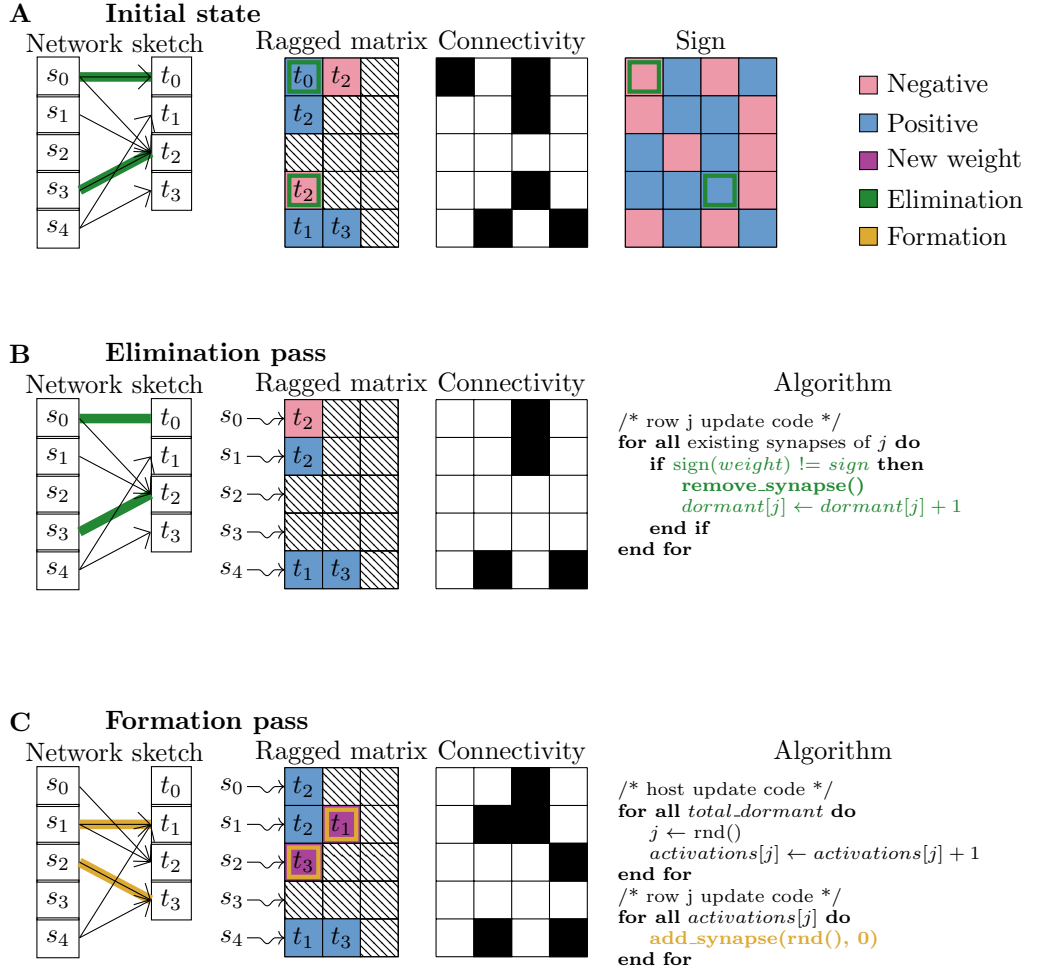


Figure 2. Illustration of data structures used for the DEEP R implementation. Five presynaptic neurons are connected to four postsynaptic neurons using sparse connectivity with a maximum out-degree of three. Each panel shows a network sketch, the ragged matrix and two bitfields – one mirroring the connectivity to provide a faster lookup and the other holding the fixed sign of each potential connection. **(A)** Initial state. Weights whose sign no longer matches the sign bit are highlighted in green. **(B)** Elimination pass. Connections highlighted in (A) are removed, the number of connections in each row made ‘dormant’ are counted and the bitfield is updated. **(C)** Formation pass. Yellow highlighting indicates new the randomly added connections.

2.1.2 DEEP R The rewiring algorithm DEEP R [25] is designed for training efficient sparse neural networks by replacing weak connections with randomly sampled new ones. DEEP R operates alongside a gradient-based learning rule and marks synapses as ‘dormant’ if weight updates would have led to weights changing sign. Dormant connections are removed and an equal number of randomly chosen synapses are added as replacements. Unlike typical incremental pruning approaches, DEEP R maintains a constant level of connection sparsity throughout training. However, like many implementations of pruning in standard ML tools, the original implementation represents the sparse connectivity as an additional dense weight matrix containing the correct sign of each connection. Here we implement a more efficient version using the structural connectivity framework described in section 2.1 which only requires two additional bitfield data structures on top of the standard GeNN sparse matrix format – one to track the sign and one the presence of each potential synaptic connection.

After the standard initialization of synaptic connectivity, a custom connectivity update is used to initialize the two additional bitfields as illustrated in figure 2A. First, all connectivity bits are cleared and all sign bits are randomized to fix the signs for all *potential* connections. Then, the update loops through all the initialized synapses in each row, sets the corresponding connectivity bit and ensures the corresponding sign bit matches the sign of the initial weight of the *actual* connection. After each training batch, DEEP R is implemented by launching a sequence of custom updates.

L1 regularisation is implemented by a custom update which adds or subtracts (based on the sign

bitfield) a constant from the gradients accumulated by e-prop to push synaptic weights towards zero.

Elimination is implemented by a custom connectivity update which loops through the synapses in each row and, if the sign of their weight does not match the sign recorded in the bitfield, removes the synapses, increments a per-row counter of ‘dormant’ synapses and clears the corresponding bit from the connectivity bitfield (figure 2A–B).

Formation is implemented by a final custom connectivity update which first uses the CPU to sum the row-wise dormant synapse count and then re-distributes these uniformly as new ‘activations’ between the rows of synaptic connectivity. Then, on the GPU, these new synapses are created for each activation, checking the connectivity bitfield to ensure there are not duplicate synapses (figure 2B–C).

In its original form [25], DEEP R also features an additional noise term but, following Bellec et al. [24] – who first combined DEEP R with e-prop – we do not include this in our implementation.

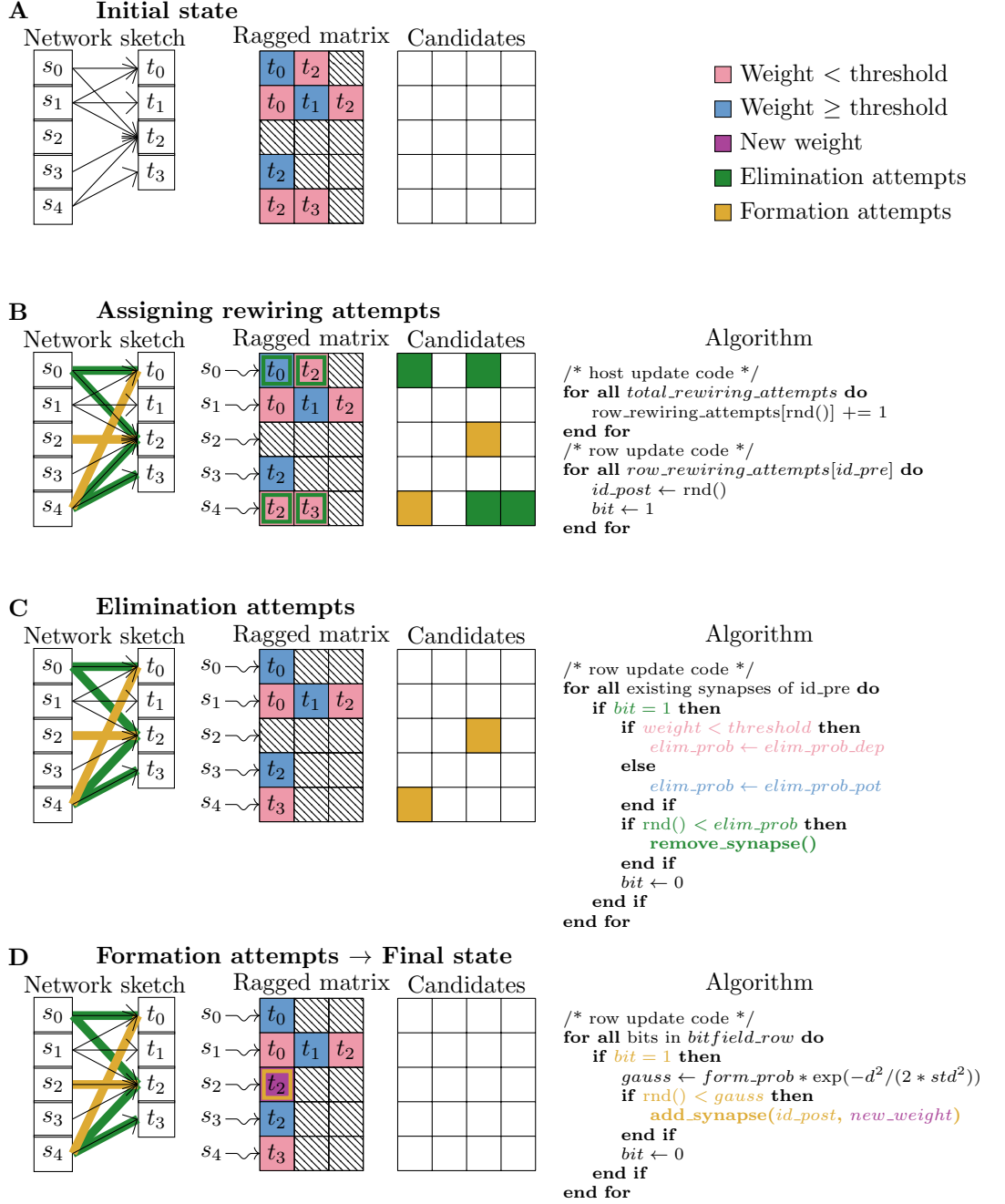


Figure 3. Illustration of data structures used for one custom connectivity update according to the synaptic rewiring model for topographic maps. Each panel shows a network sketch, the ragged matrix (number of presynaptic neurons \times maximum out-degree), the bitfield (number of presynaptic neurons \times number of postsynaptic neurons), and pseudocode. **(A)** Initial state. Five presynaptic neurons, sources s_j with $0 \leq j < 5$, are connected to four postsynaptic neurons, targets t_i with $0 \leq i < 4$, using sparse connectivity with a maximum out-degree of three. Weights below the threshold g_0 are indicated in light red, others in light blue. A synapse slot from s_j to t_i is here referred to as (s_j, t_i) . The bitfield is cleared. **(B)** Host assigns six rewiring attempts randomly to three presynaptic neurons (s_0, s_2, s_4). The presynaptic neurons then in parallel select their postsynaptic targets randomly and set the corresponding bits as candidates for rewiring attempts in the bitfield. Four existing synapses are selected for elimination (green; $(s_0, t_0), (s_0, t_2), (s_4, t_2), (s_4, t_3)$) and two empty synapse slots for formation (yellow; $(s_2, t_2), (s_4, t_0)$). **(C)** Elimination attempts. (s_0, t_0) has a low elimination probability because of the strong weight (light blue); (s_0, t_2) gets eliminated reducing the out-degree of s_0 in the ragged matrix from two to one; (s_4, t_2) gets eliminated, and the emerging gap in the row of s_4 is filled by inserting the last element t_3 ; (s_4, t_3) remains. The elimination bits get cleared in the bitfield. **(D)** Formation attempts. Assuming a spatial proximity of s_2 and t_2 and therefore a high formation probability, a new synapse (purple) is formed at (s_2, t_2) , increasing the out-degree of s_2 from zero to one, but not at (s_4, t_0) because s_4 and t_0 are farther apart. The formation bits get cleared in the bitfield.

2.1.3 Synaptic rewiring for topographic maps We develop a GeNN-compatible variation of the synaptic rewiring model proposed by Bamford, Murray, and Willshaw [28], drawing inspiration from an implementation on the SpiNNaker platform [11]. This stochastic model combines a distance-dependent formation rule with a weight-dependent removal rule. The simulation loop performs custom connectivity updates at regular intervals according to a rewiring frequency. Each update triggers a fixed number of rewiring attempts between neurons from the presynaptic and postsynaptic population. While previous implementations [28, 11] handle each rewiring attempt separately, our algorithm aims to increase efficiency by parallelizing multiple attempts. Figure 3 illustrates the hybrid CPU (host) and GPU (device) algorithm processing these attempts and highlights the data structures. First, serial host code (`host_update_code`) uniformly distributes the attempts across all neurons in the presynaptic population. As we sample with replacement, multiple attempts per presynaptic neuron are possible. In contrast to earlier implementations [28, 11], our version does not impose a fixed maximum in-degree. GeNN represents connectivity in 2D-array structures; the rows correspond to presynaptic neurons and can be operated on independently and hence in parallel. Here, we introduce a bitfield as an auxiliary structure in a similar format to mark synaptic slots between specific pre- and postsynaptic neurons for wiring attempts. On the GPU (`row_update_code`), each presynaptic neuron accesses a unique section of the bitfield with as many bits as there are neurons in the postsynaptic population. The bits therefore encode synapse slots for potential synapses between the presynaptic neuron of the row considered and all postsynaptic neurons; each bit refers to a postsynaptic neuron index. The bitfield section is initialized to zero and then as many bits are set randomly according to a uniform distribution without replacement as there are wiring attempts assigned. Each synaptic slot is therefore considered at most once, unlike the earlier versions [28, 11] where each rewiring attempt is completely independent of the others.

When the presynaptic neuron has set its bitfield row, the elimination rule is applied: A loop over all existing synapses of that presynaptic neuron identifies those that are set in the bitfield section, removes them dependent on an elimination probability compared to a random number and clears the respective bit. Weak synapses are more likely to be removed: the elimination probability is higher for depressed synapses with weights below the threshold than for strong, potentiated synapses. After all elimination attempts, the remaining set bits in the bitfield row point to synapse slots that were initially empty. Applying the formation rule, we then iterate over the whole bitfield row: If a bit is still set, we attempt to establish a synapse according to a Gaussian probability depending on the distance between the neurons and also clear that bit. The shorter the lateral distance between pre- and postsynaptic neuron, the more likely is a new connection. Our interpretation of the rewiring model does not enable the formation of multipapses (i.e., multiple synapses per neuron pair [1]). If a synapse exists, only the elimination rule is applied. To sum up, each custom connectivity update initiates a fixed number of rewiring attempts between pre- and postsynaptic neuron populations. The outcome of each attempt is a newly formed connection, a removed connection, or no change to the connectivity.

2.2 Network models

2.2.1 Recurrent classifier Our previous work [21, 22, 23] showed that recurrent SNN classifiers can be trained on datasets such as the Spiking Heidelberg Digits [39] and DVS gesture [27].

Here we train SNN classifiers with a single recurrently connected hidden layers of 512 neurons on the N-MNIST and DVS gesture datasets. Following the approach outlined by Subramoney et al. [40], we spatially downsample the DVS gesture examples from 128×128 to 32×32 resolution and temporally downsample so that there is only one spike in each 1 ms simulation timestep. When training on DVS gesture, we use adaptive LIF (ALIF) neurons, the membrane voltage (v), adaptation variable (a) and spiking output (z) of which can be described by:

$$v_j^{t+1} = \alpha (v_j^t - z_j^t v_{\text{thr}}) + \sum_{i \neq j} W_{ji}^{\text{rec}} z_i^t + \sum_i W_{ji}^{\text{in}} x_i^t \quad (1)$$

$$a_j^{t+1} = \rho a_j^t + z_j^t \quad (2)$$

$$z_j^t = H(v_j^t - (v_{\text{thr}} + \beta a_j^t)), \quad (3)$$

where $\alpha = e^{-\frac{\text{dt}}{\tau_{\text{mem}}}}$ represents the decay of the membrane with time constant $\tau_{\text{mem}} = 20$ ms, W^{rec} are the recurrent weights, W^{in} are the weights connecting the input to the recurrent layer, x^t are input spikes from the dataset, $v_{\text{thr}} = 0.6$ is the baseline spiking threshold, $\rho = e^{-\frac{\text{dt}}{\tau_{\text{adapt}}}}$ represents the adaptation variable decay with time constant $\tau_{\text{adapt}} = 2000$ ms and $\beta = 0.0174$ is the

adaptation strength. When neurons spike, v_{thr} is subtracted from their membrane voltage v . In our classifiers, W^{rec} and W^{in} are sparse and initialised with a fixed probability of connection between each pair of pre and postsynaptic neurons e.g. we use 5% connectivity to indicate that there is a 5% chance of a pair of pre and postsynaptic neurons being connected. When training on the simpler N-MNIST task, we use standard LIF neurons, the dynamics of which can be obtained by setting $\beta = 0$ and $\rho = 0$.

The network readout (y) is implemented using simple leaky integrators:

$$y_k^{t+1} = \alpha y_k^t + \sum_i W_{ki}^{\text{out}} z_j^t + b_k^{\text{out}}, \quad (4)$$

where W^{out} represents the weights connecting the hidden layer to the output and b^{out} are learned biases.

We calculate weight gradients ΔW^{rec} and ΔW^{in} using eligibility traces ϵ and e calculated using e-prop [24] (shown here for ΔW^{rec}):

$$\epsilon_{ji}^{t+1} = \psi_j^t \bar{z}_i^t + (\rho - \psi_j^t \beta) \epsilon_{ji}^t \quad (5)$$

$$e_{ji}^t = \psi_j^t (\bar{z}_i^t - \beta) \epsilon_{ji}^t \quad (6)$$

$$\Delta W_{ji}^{\text{rec}} = \sum_t \left(\sum_k B_{jk} (\pi_k^t - \pi_k^{*,t}) \right) \bar{e}_{ji}^t, \quad (7)$$

where $\psi_j^t = \frac{0.3}{v_{\text{thr}}} \max \left(0, 1 - \left| \frac{v_j^t - (v_{\text{thr}} + \beta a_j^t)}{v_{\text{thr}}} \right| \right)$ is a surrogate gradient function, \bar{z}^t is a version of z^t low-pass filtered with a time constant of τ_{mem} , η is a learning rate, $B = (W^{\text{out}})^T$, $\pi_k^t = \text{softmax}(y_1^t, \dots, y_K^t)$, $\pi^{*,t}$ are one-hot encoded labels and \bar{e}^t is a version of e^t low-pass filtered with a time constant of τ_{mem} . When using LIF neurons, only a single simpler eligibility trace is required:

$$e_{ji}^{t+1} = \psi_j^{t+1} \bar{z}_i^t \quad (8)$$

Finally, output weight gradients (ΔW^{out}) and biases (Δb^{out}) are calculated using a simple delta rule:

$$\Delta W_{kj}^{\text{out}} = \sum_t (\pi_k^t - \pi_k^{*,t}) \bar{z}_j^t \quad (9)$$

$$\Delta b_k^{\text{out}} = \sum_t (\pi_k^t - \pi_k^{*,t}). \quad (10)$$

All gradients are applied to the underlying variables using the Adam optimizer [41] and ΔW^{rec} and ΔW^{in} provide the inputs to the DEEP R algorithm described in section 2.1.2.

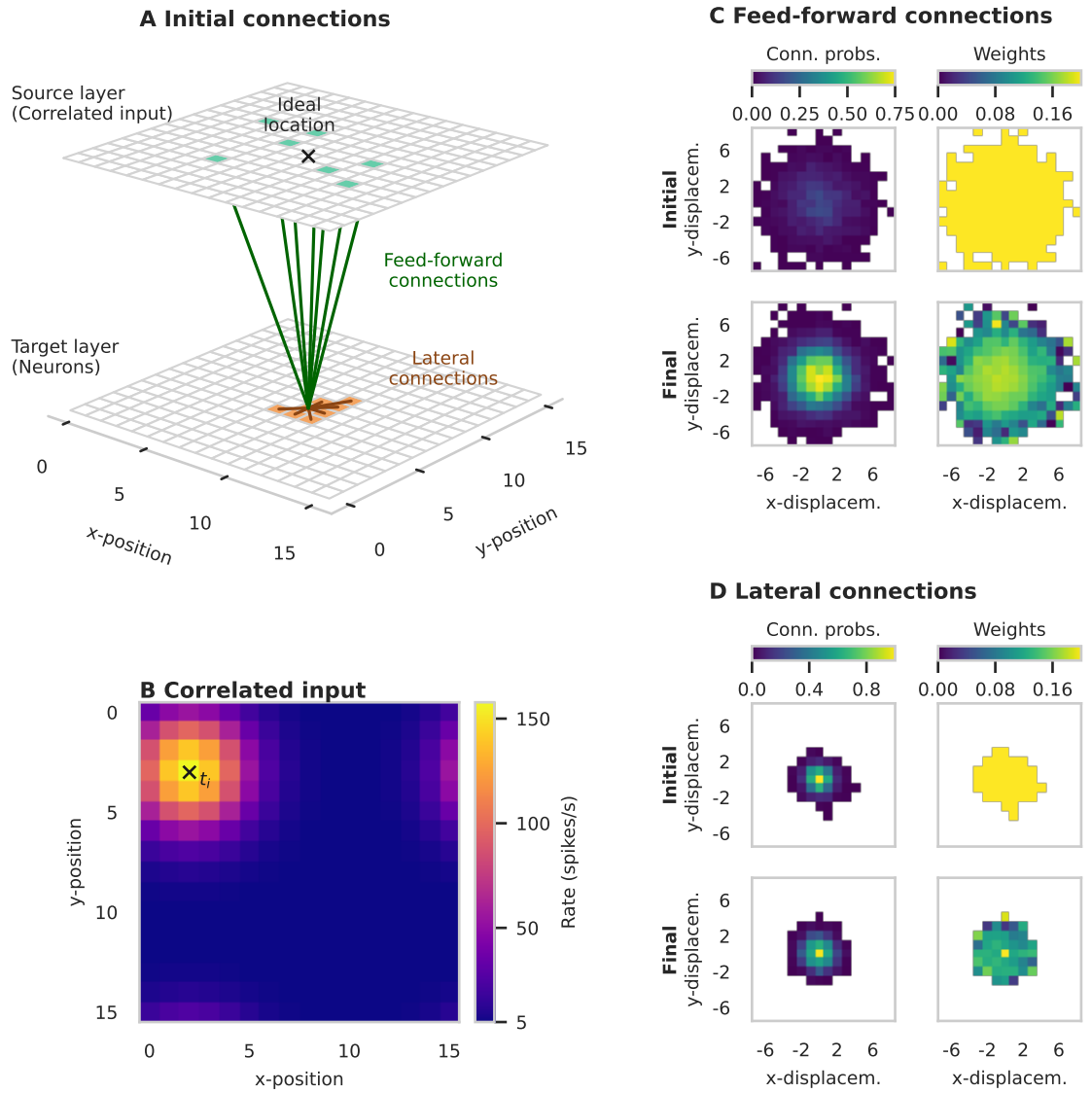


Figure 4. Topographic map model. (A) Network sketch indicating initial connections and ideal location of the preferred location for one neuron. (B) Spatially correlated input firing rates; the center (x-marker) changes in regular time intervals. Connection probabilities and weights for (C) feed-forward and (D) lateral connections, averaged over displacements for each grid position.

| A Model summary | |
|---------------------------------------|---|
| Populations | Two: source layer (Poisson inputs), target layer (excitatory neurons) |
| Topology | Nodes positioned equally spaced on square grid domain, periodic boundary conditions |
| Connectivity | Feed-forward and lateral connections, initialization with spatial profile |
| Neuron | Conductance-based leaky integrate-and-fire (LIF) |
| Input | Poisson spike trains with spatially correlated rate |
| Plasticity | Synaptic plasticity (Spike-Timing-Dependent Plasticity (STDP)), structural plasticity |
| B Neuron, input and plasticity models | |
| Neuron (target layer) | <p>Conductance-based leaky integrate-and-fire (LIF)</p> <ul style="list-style-type: none"> Membrane potential $V_i(t)$ of neuron i: Spike emission at times $t_s^i \in \mathcal{S}_i = \{t_0^i, t_1^i, t_2^i, \dots\}$ with $V_i(t_s^i) \geq V_\theta$ Subthreshold dynamics: $\tau_m \frac{dV_i}{dt} = V_{\text{rest}} - V_i + \frac{g_i}{g_{\text{leak}}} (E_{\text{exc}} - V_i) \quad \text{with} \quad g_{\text{leak}} = \frac{C_m}{\tau_m}$ if $\forall s : t \notin (t_s^i, t_s^i + \tau_{\text{ref}}]$ Reset and refractoriness: $V_i(t) = V_{\text{reset}}$ if $t \in (t_s^i, t_s^i + \tau_{\text{ref}}]$, $t_s^i \in \mathcal{S}_i$ Conductance of neuron i with presynaptic neurons j: $\tau_s \frac{dg_i}{dt} = -g_i + \sum_j g_{\text{syn},ij} \sum_s \delta(t - t_s^j - t_d)$ |
| Input (source layer) | <p>Poisson spike trains</p> <ul style="list-style-type: none"> Spatially correlated firing rate $f(i) = f_{\text{base}} + f_{\text{peak}} e^{-\frac{d_{l,i}^2}{2\sigma_{\text{stim}}^2}}$ with Euclidean distance d_{il} between stimulation center l and grid location i Stimulation center changes randomly after each interval t_{stim} |
| Synaptic plasticity | <p>Spike-Timing-Dependent Plasticity (STDP)</p> <ul style="list-style-type: none"> All-to-all spike pairing for presynaptic neuron j and postsynaptic neuron i $\frac{dg_{\text{syn},ij}}{dt} = A_+ x_j \delta(t - t_s^i) - A_- y_i \delta(t - t_s^j)$ with traces $- \frac{x_j}{\tau_+} + \sum_s \delta(t - t_s^j)$ and $\frac{dy_i}{dt} = - \frac{y_i}{\tau_-} + \sum_s \delta(t - t_s^i)$ Conductances restricted to $0 \leq g_{\text{syn}} \leq g_{\text{max}}$ |
| Structural plasticity | <p>Probabilistic connection changes with random number R sampled from uniform distribution $[0, 1)$</p> <ul style="list-style-type: none"> Activity-dependent elimination: $R < p_{\text{elim}} \text{ where } p_{\text{elim}} = \begin{cases} p_{\text{elim_dep}} & \text{for } g_{\text{syn}} < g_\theta \\ p_{\text{elim_pot}} & \text{otherwise} \end{cases}$ Distance-dependent formation: $R < p_{\text{form}} e^{-\frac{d_{ij}^2}{2\sigma_{\text{form}}^2}}$ with Euclidean distance d_{ij} between grid locations i and j, new synapse initialized with g_{max} N_{attempts} rewiring attempts after each interval t_{rewiring} |

Table 1. Topographic map model description and parameters following the guidelines of Nordlie, Gewaltig, and Plesser [42].

| C Topology | | |
|--------------------------------|---------------------------------|--|
| Symbol | Value | Description |
| L_0 | 16 | Unitless domain length at scale $s = 0$ |
| N_0 | $L_0 \times L_0 = 256$ | Network size (number of nodes per layer) at scale $s = 0$ |
| s | $\{0, \dots, 7\}$ | Scaling factor for domain length |
| D Neuron | | |
| Symbol | Value | Description |
| C_m | 20 nF | Membrane capacitance |
| τ_m | 20 ms | Membrane time constant |
| V_{rest} | -70 mV | Resting potential |
| E_{ext} | 0 mV | Reversal potential |
| V_θ | -54 mV | Firing threshold |
| V_{reset} | -70 mV | Reset potential |
| τ_{ref} | 5 ms | Absolute refractory period |
| τ_s | 5 ms | Synaptic time constant |
| t_d | 0.1 ms | Spike transmission delay |
| E Input | | |
| Symbol | Value | Description |
| f_{base} | 5 Hz | Base firing rate |
| f_{peak} | 152.8 Hz | Peak firing rate |
| σ_{stim} | 2 | Standard deviation of stimulus spread |
| t_{stim} | 20 ms | Interval for changing stimulation center |
| F Synaptic plasticity | | |
| Symbol | Value | Description |
| g_{max} | 0.2 mS | Maximum conductance |
| w_{min} | 0 mS | Minimum allowed conductance |
| w_{max} | g_{max} | Maximum allowed conductance |
| B | 1.2 | Ratio of potentiation to depression es defined in [43] |
| A_+ | $0.1 \times g_{\text{max}}$ | Learning rate for potentiation |
| τ_+ | 20 ms | Time constant for potentiation |
| τ_- | 64 ms | Time constant for depression |
| A_- | $BA_+ \frac{\tau_+}{\tau_-}$ | Learning rate for depression |
| G Structural plasticity | | |
| Symbol | Value | Description |
| $p_{\text{form-ff}}$ | 0.16 | Peak formation probability for feed-forward connections |
| $\sigma_{\text{form-ff}}$ | 2.5 | Standard deviation of receptive field for feed-forward connections |
| $p_{\text{form-lat}}$ | 1 | Peak formation probability for lateral connections |
| $\sigma_{\text{form-lat}}$ | 1 | Standard deviation of receptive field for lateral connections |
| g_θ | $\frac{1}{2} g_{\text{max}}$ | Conductance threshold |
| $p_{\text{elim-dep}}$ | $2.45 \times 10^{-2} \times 50$ | Elimination probability for depressed synapses ($g_{\text{syn}} < g_\theta$); value from [28] increased by factor |
| $p_{\text{elim-pot}}$ | $1.36 \times 10^{-4} \times 50$ | Elimination probability for potentiated synapses ($g_{\text{syn}} \geq g_\theta$); value from [28] increased by factor |
| t_{rewiring} | 1 ms | Rewiring interval |
| N_{attempts} | 10 | Number of rewiring attempts after each rewiring interval |
| H Simulation | | |
| Symbol | Value | Description |
| T_{model} | 60 s | Biological model time |
| h | 0.1 ms | Simulation time step |

Table 2. Continuation of table 1.

2.2.2 Topographic map The network model illustrated in figure 4A and its parameters closely match the earlier accounts on topographic map formation of Bamford, Murray, and Willshaw [28] and Bogdan et al. [11]. In this section, we provide a summary and emphasize the differences, while tables 1 and 2 give a complete overview of the model description and parameters used in our work in the format frequently used in computational neuroscience [42]. The model consists of two square

layers with nodes located at grid positions: model neurons in the target layer and spike-generating devices in the source layer. Feed-forward connections are established from the source to the target layer and lateral connections within the target layer. Our work is inspired by “Case 1: STDP and rewiring operating simultaneously in the presence of correlated input” of [11]. The process of creating a topographic mapping is driven by correlated input from the devices in the source layer which generate spikes with Poisson-distributed inter-spike intervals according to spatially modulated firing rates following a Gaussian decay from a stimulus center that changes location randomly in regular intervals as illustrated in figure 4B. After network initialization, both feed-forward and lateral connections are continuously updated with synaptic plasticity (i.e., weight adjustments according to an STDP rule) and structural plasticity (i.e., changes to the connectivity itself as described in section 2.1.3 in line with the “fast” rewiring protocol of [11]). Starting from a rough topographic map, simulating the model leads to a refinement of receptive fields: each neuron’s preferred location approximates its ideal location. Note that the formation rule assumes wider feed-forward than lateral connections as shown in figure 4C and D. We deviate from previous implementations [28, 11] in the following points:

- Since SpiNNaker internally scales with a maximum weight, we multiply the STDP learning rate A_+ given in their table 1 with their g_{\max} to get the same effect.
- Instead of nearest-neighbor spike pairing, we use all-to-all pairing of pre- and postsynaptic spikes to compute the weight updates of the STDP model [2].
- We also use the formation rule to initialize the connectivity, but instead of fixing the initial in-degree, we apply the “pairwise Bernoulli” rule [1] using probabilities computed according to the formation probability given in table 1. This approach leads to on average $K = 2\pi p_{\text{form}}\sigma_{\text{form}}$ synapses per neuron instead of 32 and excludes multapses [1] from the beginning as these are not supported by the structural plasticity rule.
- To keep the formation and elimination in balance without fixing the maximum in-degree, we increase both of the elimination probabilities $p_{\text{elim_dep}}$ and $p_{\text{elim_pot}}$ by a factor of 50.
- Our rewiring attempts are executed in parallel for each presynaptic neuron instead of sequentially.
- We use a simulation time step of $h = 0.1$ ms (same as [28]) in contrast to 1 ms [11] and solve the neuron dynamics with the exponential Euler method. Our delay also corresponds to one time step.

Going beyond the network size used in the original model, we scale the domain length L_0 with an integer scaling factor s . To preserve the dynamics, we replicate the correlated input in each added square such that there are s^2 stimulus locations selected simultaneously in each stimulation interval. The number of rewiring attempts in the full network is also scaled with s^2 . For inspecting the connectivity evolution, we read out the connectivity after each connectivity update which slows down the simulation; for performance measurements we do not do such readouts.

2.3 Software and hardware summary

Topographic map model simulations are performed on one GPU of an NVIDIA DGX A100 system using GeNN 5.3.0 and Python 3.12.3. DEEP R training was performed on the JUWELS Booster HPC system, using an environment with Python 3.11.3, GeNN 5.2.0 and mlGeNN 2.4.0. All analysis and plotting uses Python with numpy 1.26.4, and matplotlib 3.8.4. All source codes to reproduce our results are publicly available on GitHub (https://github.com/jhmsnk/genn_structural_plasticity).

3 Results

3.1 Classification with DEEP R

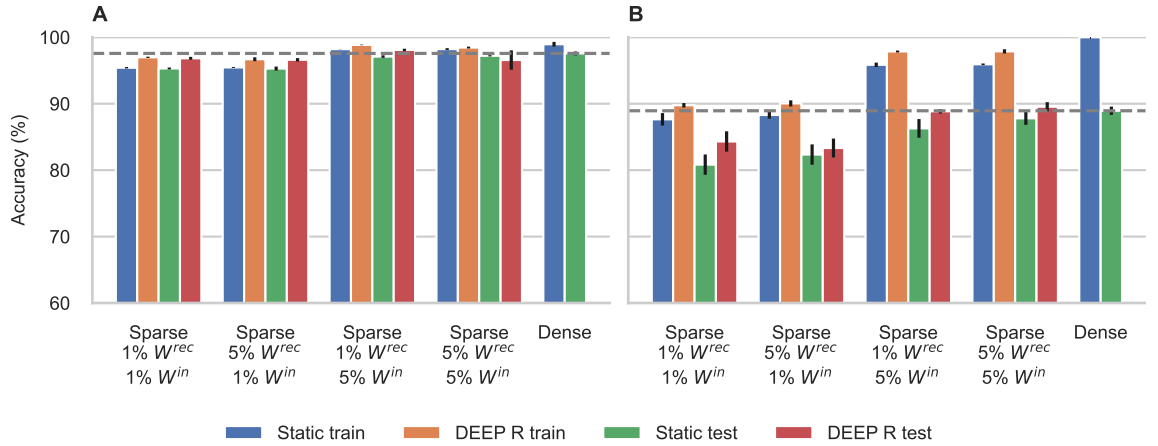


Figure 5. Classification accuracy. Bar heights show mean accuracy and error bars standard deviations, all calculated over five repeats with different seeds. The dashed line shows the mean test accuracy of the baseline dense network. (A) N-MNIST. (B) DVS-gesture.

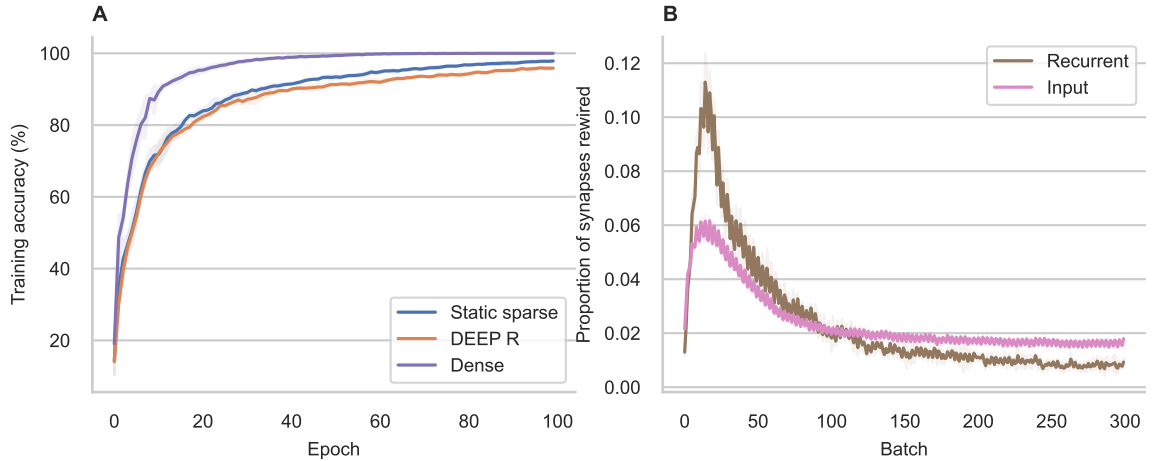


Figure 6. DVS gesture training dynamics. Lines show mean values and shaded areas indicate one standard deviation, all calculated over five repeats with different seeds. Sparse models have 5% W^{in} connectivity and 1% W^{rec} connectivity. (A) Training convergence. (B) DEEP R rewiring. Proportion of synapses rewired over the course of training.

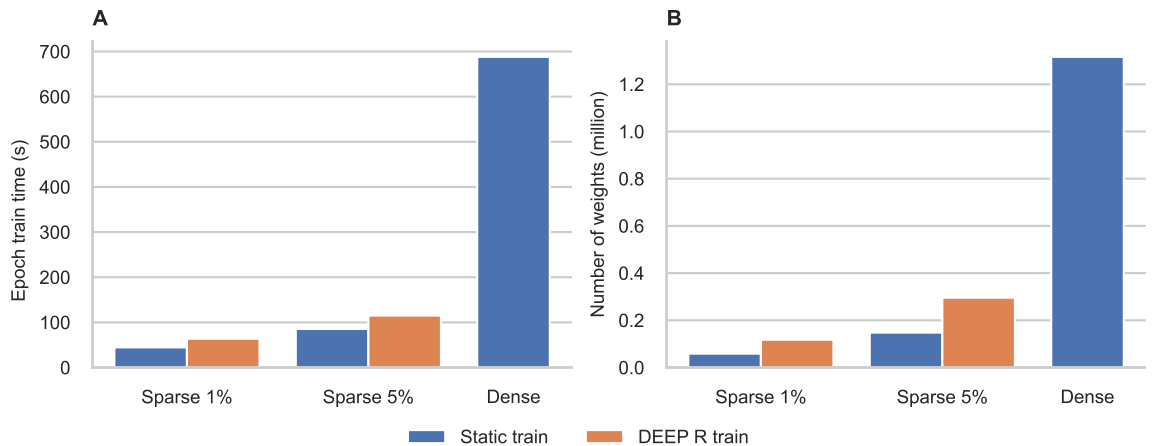


Figure 7. Performance and weight savings of sparse DVS gesture training. Sparse models shown have the same sparsity in W^{in} and W^{rec} . (A) Training time. (B) The number of weights in models.

Figure 5 shows the training and testing accuracy of sparse and dense classifier networks (section 2.2.1) trained on the N-MNIST [26] and DVS gesture dataset [27] using mlGeNN (see section 2.1.1) with the GPU-parallelised DEEP R implementation described in section 2.1.2. We trained all models for 100 epochs using a batch size of 512 and the Adam optimizer [41] with default parameters. We also used the default e-prop parameters for all networks only optimizing the L1 regularization strength on a validation set. Neither dataset contains a dedicated validation split so, as N-MNIST has a large number of examples, we simply held out 10000 random examples whereas, for DVS gesture, we employed a cross-validation methodology – where we leave out two users in each fold (after Nowotny, Turner, and Knight [21]).

Except for the model trained on DVS gesture with 5% input connectivity and 1% recurrent connectivity; and the model trained on N-MNIST with 5% input connectivity and 5% recurrent connectivity, using DEEP R significantly improves the performance of all sparse models compared to the versions trained with fixed connectivity ($p < 0.05$, paired, one-sided Wilcoxon signed rank test [44], $n = 5$). Furthermore, as long as there are sufficiently many input connections ($\geq 5\%$ input connectivity), sparse models trained with DEEP R matched the performance of the dense reference networks on both datasets. Specifically, our models with 5% input connectivity and 1% recurrent connectivity trained on DVS gesture obtains a test accuracy of $88.86 \pm 0.3\%$ compared to $88.94 \pm 0.6\%$ for the dense model. This is higher than the 88.0% reported by Subramoney et al. [40] for an event-based Gated Recurrent Unit (GRU) model and is achieved with around $90\times$ fewer parameters (60×10^3 vs. 5.5×10^6).

Figure 6A shows the training dynamics of three types of models on the DVS gesture dataset and demonstrates that the training of all types is stable, although, as the literature predicts, the sparser models train more slowly [45]. Figure 6B shows how the rate of DEEP R rewiring changes over time with drastic changes in connectivity happening during the first 100 batches but connectivity remaining more or less unchanged towards the end of training, matching the intuition that DEEP R is sampling network connectivity and then settling into a possible solution.

We then measured computational speed of DVS gesture training. As shown in figure 7A, training models with 5% connectivity using e-prop and GeNN is up to $8\times$ faster than training a dense model and training models with 1% connectivity is up to $15\times$ faster. While the time spent running the DEEP R updates described in section 2.1.2 takes a maximum of 0.5% of the total training time, training the models with DEEP R is slightly slower because we (conservatively) double the maximum out-degree in the ragged sparse matrix data structure (see section 2.1) to allow space for rewiring. Figure 7B shows the number of weights in each model configuration. Due to the padding, the number of weights and hence memory savings are not directly proportional to the sparsity. Nonetheless, DEEP R models with 1% connectivity still require $11\times$ fewer weights than if they were implemented using dense matrices and those with 5% connectivity $4\times$ fewer.

Overall, in GeNN, connection sparsity significantly reduces training times and memory usage. This represents a significant advantage compared to SNN simulation libraries such as SNNtorch [32], NORSE [33] or JAXsnn [34] which are built on standard Machine Learning toolkits like PyTorch or JAX and thus only provide efficient support for dense weight matrices.

Feed-forward connections

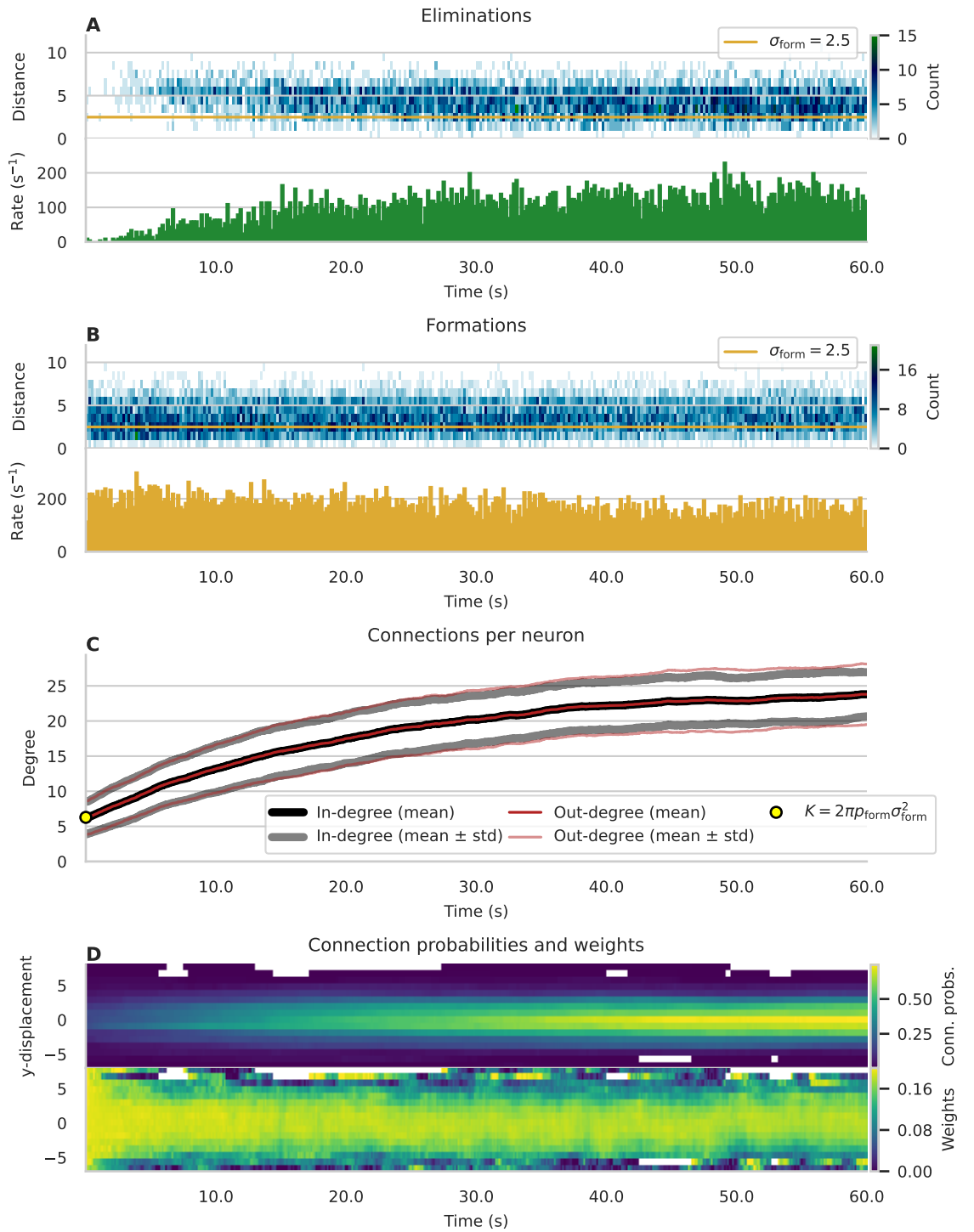


Figure 8. Evolution of feed-forward connections in topographic map model. (A) Eliminations. Top: Color-coded count of removed connections at given spatial separation in time bins of 200 ms and spatial bins of 1 unit. Standard deviation of the Gaussian-shaped formation probability σ_{form} indicated by yellow line. Bottom: Histogram of elimination rate using time bins of 200 ms. (B) Formations. Same display as in (A). (C) In-degree (black) and out-degree (red); mean values (dark) and mean \pm standard deviation (light). Theoretical estimate for initial degree indicated by circular marker. (D) Connection probabilities and weights for zero x-displacement. Initial and final frames correspond to figure 4C.

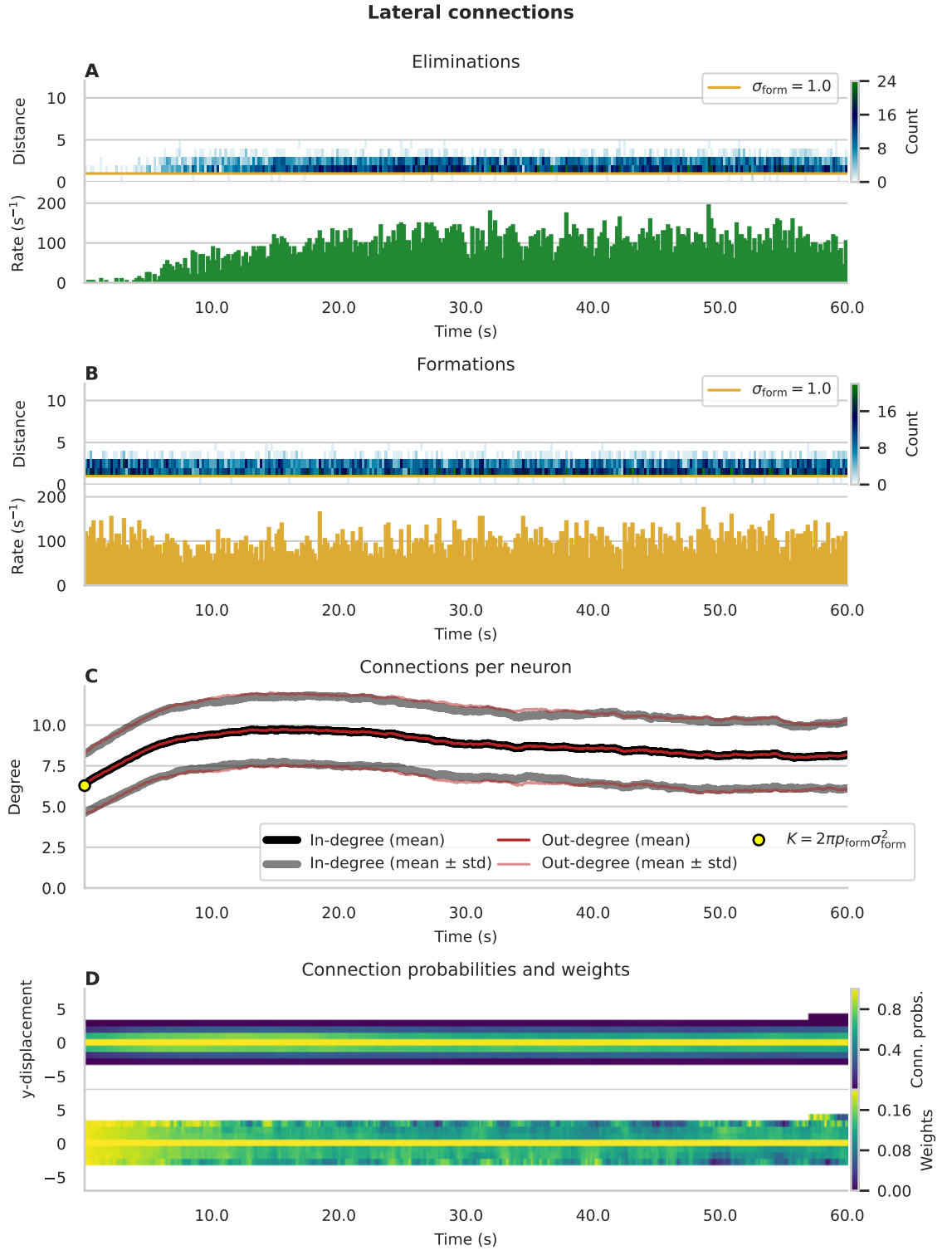


Figure 9. Evolution of lateral connections in topographic map model. (A)–(D) Same display as in figure 8. Initial and final frames in panel (D) correspond to figure 4D.

3.2 Topographic map formation

Figures 8 and 9 show the evolution of feed-forward and lateral connections, respectively. Following the rough topographic map initialization according to the formation probability given in table 1, the elimination rate gradually increases and then stabilizes, while the formation rate is mostly stable over the time course of the simulation, see panels A and B. The increased elimination probabilities in our implementation compared to [28] result in similar elimination and formation rates after the initial warm-up phase without the need for fixing the maximum in-degree. These rates are higher for the feed-forward than for the lateral connections due to the higher standard deviation of the

Gaussian-shaped formation probability. In particular in the beginning of the simulation, it can be observed that connections established across larger distances get predominantly eliminated because the synaptic plasticity weakens these synapses triggered by the spatially correlated Poisson input. Note that the upper displays of panels A and B only count the changes in connectivity at certain spatial separations of the respective grid locations without taking into account the number of possible connections per distance. For instance, there is only one grid position at zero distance (for lateral connections this corresponds to autapses [1]) and four grid positions at a distance of one. Panel C shows how the connections per neuron evolve on average. The results for in-degrees and out-degrees are similar. The starting point matches the theoretical expectation, and it is the same for feed-forward and lateral because in both cases the parameters are chosen such that $p_{\text{form}}\sigma_{\text{form}} = 1$. From this starting point, the number of feed-forward connections per neuron grows until saturation. In contrast, the number of lateral connections decreases after an initial increase until reaching a stable value. While figure 4C and D show connection probabilities and weights averaged over displacements for each grid position just for the initial and final state, panel D of figures 8 and 9 illustrate the temporal evolution across all y-displacements with zero x-displacement. The gradual refinement of the receptive fields is visible mostly close to the ideal location. In more distant places new synapses get formed, but their weights decrease from their high initial value due to the normal synaptic weight plasticity, and they get eventually eliminated again.

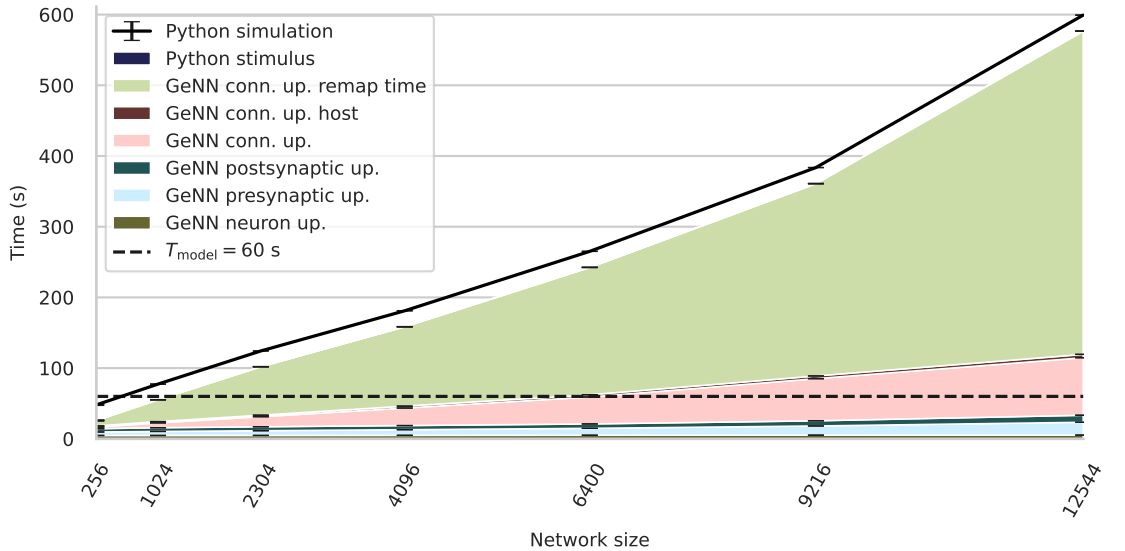


Figure 10. Scaling performance of topographic map model. Measured wall-clock time of simulations with network sizes increasing from scale $s = 1$ ($16 \times 16 = 256$ neurons) to $s = 7$ ($112 \times 112 = 12,544$ neurons); averages over three random seeds. Total simulation time measured on the Python level (black curve) and stacked, color-coded contributions resolved with GeNN built-in timers and a Python-level timer for updating the stimulus center location of the correlated input. Realtime indicated by black dashed line.

We then measure the computational speed of the implementation. The runtime for increasing network sizes is illustrated in figure 10. At the network size used in the original publication [28] ($s = 1$) we observe faster-than-realtime performance with the GeNN implementation. Even though the measured wall-clock time increases when increasing the network size, the proportionality factor is smaller than one: For example, at $s = 7$ the network size grows by a factor of 49, but the simulation time only by ca. 10. The largest contributions to the total runtime are in fact due to the connectivity updates, in particular the time for remapping the inverse ragged matrix, followed by the update on the device required for STDP, while the time for the host update is negligible. The number of successful rewiring attempts remains constant when increasing the network size because the formation rule only establishes local connections. In contrast, the total number of rewiring attempts increases with the network size but is performed in parallel. Neuron and synapse updates (i.e., presynaptic and postsynaptic, including synaptic plasticity), and the Python code to switch the stimulus center location of the correlated input are also comparatively insignificant for larger network sizes. The gap between the sum of individual contributions and the total simulation time measured on the Python level is most likely due to the overheads of Python calling C++.

4 Discussion

We propose a flexible and efficient structural plasticity framework for the GeNN simulator which addresses the challenges of parallelizing structural plasticity algorithms and handles their complex dependencies on other neuronal and synaptic mechanisms, while minimizing the computational cost of changing connectivity in allocated data structures. We demonstrate this framework using two different applications: In a spike-based ML context, we train recurrent classifiers with very sparse connectivity using supervised learning and the DEEP R structural plasticity rule. In a computational neuroscience context, we show unsupervised learning leading to the refinement of a topographic map using a structural plasticity rule with activity-dependent and activity-independent contributions.

The ‘lottery ticket hypothesis’[45] states that, within dense networks, there exist sparse sub-networks (the winning tickets) which can be trained in isolation to obtain the same test accuracy as the dense network in the same number of epochs. On this basis, the sparse classifiers we trained using DEEP R appear to be promising winning tickets as they maintain the same performance as networks with dense connectivity, even though they are extremely sparse: each hidden neuron only has around 5 outgoing recurrent synapses and each input only around 25 feed-forward synapses. However, as figure 6A shows, these potential winning tickets converge more slowly than the dense networks. This reduced convergence speed could be due to ‘competition’ between e-prop learning, L1 regularization and the rewiring process (which occurs every batch) and it would be interesting to explore this further by retaining the connectivity structure of the sparse networks trained using DEEP R, reinitializing their weights and retraining them from scratch while keeping the connectivity static. Evci et al. [46] found that forming new connections randomly – as DEEP R does – limits the performance of sparse networks and propose using gradients from *potential* synapses to guide where new synapses are formed. While this approach is impossible in a truly sparse framework such as we are developing here, it would be interesting to combine DEEP R with more biologically-inspired ‘guidance’ such as the distance-dependent formation rule used in the topographic map formation model (table 1). Additionally, exploring how different tasks affect the efficacy of DEEP R and whether it can be combined with more efficient learning rules such as Eventprop [38, 21] would both be interesting future directions for this work.

Using the novel structural plasticity framework, we have implemented a variation of the structural plasticity mechanism proposed by Bamford, Murray, and Willshaw [28] which includes an interplay between structural plasticity, synaptic plasticity and spatial inter-neuron distance dependence. The mechanism promotes a refinement of receptive fields in a topographic map model [28] compatible with the results of [11]. Our analysis reveals further insights into the time course of synapse formation and elimination, in particular the feasibility of compensating for not fixing the maximum in-degree by adjusting the elimination probabilities. While the SpiNNaker implementation [11] achieves realtime performance with a simulation time-step of $h = 1$ ms, GeNN demonstrates faster-than-realtime performance despite using a $10\times$ smaller time step. In contrast to previous implementations, the GeNN model applies multiple rewiring attempts in parallel, and demonstrates the scaling performance on a GPU upon upscaling the network size. At the original size, 10 rewiring attempts are performed in parallel and at the largest tested size $10 \times 49 = 490$. Other synaptic plasticity rules that involve more inherent parallelism would benefit even more from this feature. Both the structural plasticity mechanism and the network model used to demonstrate topographic map refinement serve as proofs-of-concept for the technological capability rather than claiming full biological realism. Bamford, Murray, and Willshaw [28] and Bogdan et al. [11] provide extensive discussions on the limitations and on potential improvements, for example, axon branching could be guided by the existence of axons, homeostatic mechanisms could avoid the need for new synapses to start strong, and more realistic inputs, distance-dependent delays and inhibition could be added. Any biological interpretation of our example results should take the simplifications of the current approach into account.

The performance impact of structural plasticity updates on the two models we simulate is drastically different. In our e-prop classifier models, DEEP R only adds a 0.5% overhead to training time whereas, when simulating large topographic map models (scale $s = 7$), structural plasticity updates account for around 90% of the simulation time. There are numerous reasons for this. Firstly, DEEP R is only run after each batch (18456 timesteps for DVS-gesture) whereas the refinement rule used in the topographic map model is run much more frequently (every 10 timesteps). Additionally, in each of these batches, 512 model instances are updated in parallel further amortizing the cost of the DEEP R updates. The final issue is the large ‘remap time’ seen in figure 10 (see section 2.1). Because, only around 50% of connectivity updates in the topographic map model result in connection changes, one easy optimisation would be to only perform the

remapping process if the connectivity has actually changed. Furthermore, more efficient GPU STDP implementations have been recently developed [47] which do not require this type of data structure at all. However, incorporating further optimisations into GeNN is beyond the scope of this paper and, while these overheads may limit the practicability of our approach for large models using STDP with a postsynaptic spike-triggered term, the performance impact of structural plasticity will be minimal for many other models.

This study demonstrates the feasibility of expressing different structural plasticity rules [28, 25] using the syntax of our novel structural plasticity framework and enabling efficient GPU-based simulations of network dynamics. We hope that the proposed framework serves as a useful tool to support further explorations of biologically founded structural plasticity mechanisms and their exploitation for spike-based ML. While we have not explored it here, this framework could also be used to implement neurogenesis by instantiating the final number of neurons at the start of the simulation without any synaptic connections and connecting them over time. This approach has been widely used to implement neurogenesis both in software simulators [48] and neuromorphic hardware [49].

Despite considering generic challenges of structural plasticity implementations, our design is tailored towards GPU-based systems and in particular the GeNN simulator. However, such frameworks are potentially applicable to other simulation software that uses code generation such as Brian 2 [50] or NESTML [51] as well as programmable neuromorphic hardware. For example, ongoing work [52] to target the SpiNNaker [17] and SpiNNaker 2 [53] neuromorphic systems using NESTML would provide an interesting route for running flexible structural plasticity rules at scale. Furthermore, both Loihi [54] and BrainScaleS-2 [18] supports sparse connectivity and, potentially, code could be generated to run on the general processors present in both systems to modify this connectivity. Accelerated-time systems such as BrainScaleS-2 would be a particularly interesting choice for implementing structural plasticity as they can overcome the long simulation times otherwise required to simulate the slow speed of structural changes in biology.

Acknowledgements

This project has received funding from EPSRC (grant numbers EP/V052241/1 to JK and EP/S030964/1 to TN and JK), the European Union’s Horizon 2020 Framework Programme for Research and Innovation under Specific Grant Agreement No. 945539 (Human Brain Project SGA3) to TN and JS, the European Union’s Horizon Europe Programme under the Specific Grant Agreement No. 101147319 (EBRAINS 2.0 Project) to JS, and the VolkswagenStiftung under the "STRUCTICITY: Multi-level STRUCTure and plASTICITY in large-scale spiking neural networks for event-based sensing" project (9D558/-1) to JS.

Compute time was provided through Gauss Centre for Supercomputing application number 21018 and EPSRC (grant number EP/T022205/1) and local GPU hardware was provided by an NVIDIA hardware grant award.

Johanna Senk is grateful to the Institute for Advanced Simulation (IAS-6), Jülich Research Centre, for making a research visit at the University of Sussex possible during which this project has been started, and for providing access to their NVIDIA DGX A100 system used partially for the research performed.

References

- [1] Johanna Senk et al. “Connectivity concepts in neuronal network modeling.” *PLOS Computational Biology* 18.9 (2022). Ed. by Roberto Toro, e1010086. DOI: [10.1371/journal.pcbi.1010086](https://doi.org/10.1371/journal.pcbi.1010086).
- [2] A. Morrison, M. Diesmann, and W. Gerstner. “Phenomenological models of synaptic plasticity based on spike-timing.” *Biological Cybernetics* 98.6 (2008), pp. 459–478. DOI: [10.1007/s00422-008-0233-1](https://doi.org/10.1007/s00422-008-0233-1).
- [3] Michael Fauth and Christian Tetzlaff. “Opposing Effects of Neuronal Activity on Structural Plasticity.” *Frontiers in Neuroanatomy* 10 (2016). DOI: [10.3389/fnana.2016.00075](https://doi.org/10.3389/fnana.2016.00075).
- [4] Joseph Altman and Gopal D. Das. “Autoradiographic and histological evidence of postnatal hippocampal neurogenesis in rats.” *Journal of Comparative Neurology* 124.3 (1965), 319–335. DOI: [10.1002/cne.901240303](https://doi.org/10.1002/cne.901240303).
- [5] Gerd Kempermann et al. “Human Adult Neurogenesis: Evidence and Remaining Questions.” *Cell Stem Cell* 23.1 (2018), 25–30. DOI: [10.1016/j.stem.2018.04.004](https://doi.org/10.1016/j.stem.2018.04.004).
- [6] Trevor Gale, Erich Elsen, and Sara Hooker. *The State of Sparsity in Deep Neural Networks*. 2019. arXiv: [1902.09574\[cs, stat\]](https://arxiv.org/abs/1902.09574).

- [7] Marcus Frean. “The Upstart Algorithm: A Method for Constructing and Training Feedforward Neural Networks.” *Neural Computation* 2.2 (1990), 198–209. DOI: [10.1162/neco.1990.2.2.198](https://doi.org/10.1162/neco.1990.2.2.198).
- [8] Tin-Yau Kwok and Dit-Yan Yeung. “Constructive algorithms for structure learning in feedforward neural networks for regression problems.” *IEEE Transactions on Neural Networks* 8.3 (1997), 630–645. DOI: [10.1109/72.572102](https://doi.org/10.1109/72.572102).
- [9] Sandra Diaz-Pier et al. “Automatic Generation of Connectivity for Large-Scale Neuronal Network Models through Structural Plasticity.” *Frontiers in Neuroanatomy* 10 (2016). DOI: [10.3389/fnana.2016.00057](https://doi.org/10.3389/fnana.2016.00057).
- [10] Richard George, Giacomo Indiveri, and Stefano Vassanelli. “Activity dependent structural plasticity in neuromorphic systems.” *2017 IEEE Biomedical Circuits and Systems Conference (BioCAS)*. IEEE, 2017. DOI: [10.1109/biocas.2017.8325074](https://doi.org/10.1109/biocas.2017.8325074).
- [11] Petruț A Bogdan et al. “Structural Plasticity on the SpiNNaker Many-Core Neuromorphic System.” *Frontiers in Neuroscience* 12.12 (2018), pp. 1–20. DOI: [10.3389/fnins.2018.00434](https://doi.org/10.3389/fnins.2018.00434).
- [12] Chen Liu et al. “Memory-Efficient Deep Learning on a SpiNNaker 2 Prototype.” *Frontiers in Neuroscience* 12 (2018). DOI: [10.3389/fnins.2018.00840](https://doi.org/10.3389/fnins.2018.00840).
- [13] Sebastian Rinke et al. “A Scalable Algorithm for Simulating the Structural Plasticity of the Brain.” *Journal of Parallel and Distributed Computing* 120 (2018), pp. 251–266. DOI: [10.1016/j.jpdc.2017.11.019](https://doi.org/10.1016/j.jpdc.2017.11.019).
- [14] Yexin Yan et al. “Efficient Reward-Based Structural Plasticity on a SpiNNaker 2 Prototype.” *IEEE Transactions on Biomedical Circuits and Systems* 13.3 (2019), 579–591. DOI: [10.1109/tbcas.2019.2906401](https://doi.org/10.1109/tbcas.2019.2906401).
- [15] Sebastian Billaudelle et al. “Structural plasticity on an accelerated analog neuromorphic hardware system.” *Neural Networks* 133 (2021), 11–20. DOI: [10.1016/j.neunet.2020.09.024](https://doi.org/10.1016/j.neunet.2020.09.024).
- [16] Julien Vitay, Helge Ü. Dinkelbach, and Fred H. Hamker. “ANNarchy: a code generation approach to neural simulations on parallel hardware.” *Frontiers in Neuroinformatics* 9 (July 2015), pp. 1–20. DOI: [10.3389/fninf.2015.00019](https://doi.org/10.3389/fninf.2015.00019). arXiv: [1702.06463](https://arxiv.org/abs/1702.06463).
- [17] Stephen B Furber et al. “The SpiNNaker Project.” *Proceedings of the IEEE* 102.5 (2014), pp. 652–665. DOI: [10.1109/JPR0C.2014.2304638](https://doi.org/10.1109/JPR0C.2014.2304638).
- [18] Christian Pehle et al. “The BrainScaleS-2 Accelerated Neuromorphic System With Hybrid Plasticity.” *Frontiers in Neuroscience* 16 (2022), p. 795876. DOI: [10.3389/fnins.2022.795876](https://doi.org/10.3389/fnins.2022.795876).
- [19] Esin Yavuz, James Turner, and Thomas Nowotny. “GeNN: a code generation framework for accelerated brain simulations.” *Scientific Reports* 6.1 (2016). Publisher: Nature Publishing Group, p. 18854. DOI: [10.1038/srep18854](https://doi.org/10.1038/srep18854).
- [20] James C Knight, Anton Komissarov, and Thomas Nowotny. “PyGeNN: A Python Library for GPU-Enhanced Neural Networks.” *Frontiers in Neuroinformatics* 15.April (2021). DOI: [10.3389/fninf.2021.659005](https://doi.org/10.3389/fninf.2021.659005).
- [21] Thomas Nowotny, James P Turner, and James C Knight. “Loss shaping enhances exact gradient learning with Eventprop in spiking neural networks.” *Neuromorphic Computing and Engineering* 5.1 (2025), p. 014001. DOI: [10.1088/2634-4386/ada852](https://doi.org/10.1088/2634-4386/ada852).
- [22] James C Knight and Thomas Nowotny. “Efficient GPU training of LSNNs using eProp.” *Neuro-Inspired Computational Elements Conference*. New York, NY, USA: ACM, 2022, pp. 8–10. DOI: [10.1145/3517343.3517346](https://doi.org/10.1145/3517343.3517346).
- [23] James C Knight and Thomas Nowotny. “Easy and efficient spike-based Machine Learning with mlGeNN.” *Neuro-Inspired Computational Elements Conference*. San Antonio TX USA: ACM, 2023, pp. 115–120. DOI: [10.1145/3584954.3585001](https://doi.org/10.1145/3584954.3585001).
- [24] Guillaume Bellec et al. “A solution to the learning dilemma for recurrent networks of spiking neurons.” *Nature Communications* 11.1 (2020), p. 3625. DOI: [10.1038/s41467-020-17236-y](https://doi.org/10.1038/s41467-020-17236-y).
- [25] Guillaume Bellec et al. *Deep rewiring: Training very sparse deep networks*. arXiv: 1711.05136. 2018.
- [26] Garrick Orchard et al. “Converting static image datasets to spiking neuromorphic datasets using saccades.” *Frontiers in Neuroscience* 9 (NOV 2015), pp. 1–11. DOI: [10.3389/fnins.2015.00437](https://doi.org/10.3389/fnins.2015.00437). arXiv: [1507.07629](https://arxiv.org/abs/1507.07629).

- [27] Arnon Amir et al. “A Low Power, Fully Event-Based Gesture Recognition System.” *2017 IEEE Conference on Computer Vision and Pattern Recognition (CVPR)*. ISSN: 1063-6919. IEEE, 2017, pp. 7388–7397. DOI: [10.1109/CVPR.2017.781](https://doi.org/10.1109/CVPR.2017.781).
- [28] Simeon a Bamford, Alan F Murray, and David J Willshaw. “Synaptic rewiring for topographic mapping and receptive field development.” *Neural networks : the official journal of the International Neural Network Society* 23.4 (2010). Publisher: Elsevier Ltd, pp. 517–27. DOI: [10.1016/j.neunet.2010.01.005](https://doi.org/10.1016/j.neunet.2010.01.005).
- [29] NVIDIA, Péter Vingelmann, and Frank H.P. Fitzek. *CUDA, developer.nvidia.com/cuda-toolkit*. 2020.
- [30] Advanced Micro Devices. *AMD HIP Programming Guide*. 2021.
- [31] Wenzel Jakob, Jason Rhinelander, and Dean Moldovan. *pybind11 — Seamless operability between C++11 and Python*. 2016.
- [32] Jason K Eshraghian et al. “Training spiking neural networks using lessons from deep learning.” *Proceedings of the IEEE* 111.9 (2023), pp. 1016–1054.
- [33] Christian Pehle and Jens Egholm Pedersen. *Norse - A deep learning library for spiking neural networks*. Version 0.0.7. Documentation: <https://norse.ai/docs/>. 2021. DOI: [10.5281/zenodo.4422025](https://doi.org/10.5281/zenodo.4422025).
- [34] Eric Müller et al. *jaxsnn: Event-driven Gradient Estimation for Analog Neuromorphic Hardware*. 2024. arXiv: [2401.16841](https://arxiv.org/abs/2401.16841) [cs].
- [35] Markus Butz and Arjen van Ooyen. “A Simple Rule for Dendritic Spine and Axonal Bouton Formation Can Account for Cortical Reorganization after Focal Retinal Lesions.” *PLoS Computational Biology* 9.10 (2013), pp. 39–43. DOI: [10.1371/journal.pcbi.1003259](https://doi.org/10.1371/journal.pcbi.1003259).
- [36] James C. Knight and Thomas Nowotny. “GPUs Outperform Current HPC and Neuromorphic Solutions in Terms of Speed and Energy When Simulating a Highly-Connected Cortical Model.” *Frontiers in Neuroscience* 12 (December 2018), pp. 1–19. DOI: [10.3389/fnins.2018.00941](https://doi.org/10.3389/fnins.2018.00941).
- [37] James Paul Turner et al. “mlGeNN: accelerating SNN inference using GPU-enabled neural networks.” *Neuromorphic Computing and Engineering* 2.2 (2022). Publisher: IOP Publishing, p. 024002. DOI: [10.1088/2634-4386/ac5ac5](https://doi.org/10.1088/2634-4386/ac5ac5).
- [38] Timo C Wunderlich and Christian Pehle. “Event-based backpropagation can compute exact gradients for spiking neural networks.” *Scientific Reports* 11.1 (2021), p. 12829. DOI: [10.1038/s41598-021-91786-z](https://doi.org/10.1038/s41598-021-91786-z).
- [39] Benjamin Cramer et al. “The Heidelberg Spiking Data Sets for the Systematic Evaluation of Spiking Neural Networks.” *IEEE Transactions on Neural Networks and Learning Systems* (2022). arXiv: 1910.07407, pp. 1–14. DOI: [10.1109/TNNLS.2020.3044364](https://doi.org/10.1109/TNNLS.2020.3044364).
- [40] Anand Subramoney et al. “Efficient recurrent architectures through activity sparsity and sparse back-propagation through time.” *The Eleventh International Conference on Learning Representations*. 2023.
- [41] Diederik P Kingma and Jimmy Lei Ba. “Adam: A method for stochastic optimization.” *3rd International Conference on Learning Representations, ICLR 2015 - Conference Track Proceedings*. 2015, pp. 1–15. arXiv: [1412.6980](https://arxiv.org/abs/1412.6980).
- [42] Eilen Nordlie, Marc-Oliver Gewaltig, and Hans Ekkehard Plesser. “Towards Reproducible Descriptions of Neuronal Network Models.” *PLoS Computational Biology* 5.8 (2009). Ed. by Karl J. Friston, e1000456. DOI: [10.1371/journal.pcbi.1000456](https://doi.org/10.1371/journal.pcbi.1000456).
- [43] Sen Song and L.F. Abbott. “Cortical Development and Remapping through Spike Timing-Dependent Plasticity.” *Neuron* 32.2 (2001), 339–350. DOI: [10.1016/s0896-6273\(01\)00451-2](https://doi.org/10.1016/s0896-6273(01)00451-2).
- [44] Frank Wilcoxon. “Individual comparisons by ranking methods.” *Biometrics bulletin* 1.6 (1945), pp. 80–83.
- [45] Jonathan Frankle and Michael Carbin. *The Lottery Ticket Hypothesis: Finding Sparse, Trainable Neural Networks*. 2019. DOI: [10.48550/arXiv.1803.03635](https://doi.org/10.48550/arXiv.1803.03635). arXiv: [1803.03635](https://arxiv.org/abs/1803.03635) [cs].
- [46] Utku Evci et al. “Rigging the Lottery: Making All Tickets Winners.” *Proceedings of the 37th International Conference on Machine Learning*. International Conference on Machine Learning. PMLR, 2020, pp. 2943–2952.

- [47] Dennis Bautembach, Iason Oikonomidis, and Antonis Argyros. “Even Faster SNN Simulation with Lazy+Event-driven Plasticity and Shared Atomics.” *2021 IEEE High Performance Extreme Computing Conference (HPEC)*. 2021 IEEE High Performance Extreme Computing Conference (HPEC). ISSN: 2643-1971. 2021, pp. 1–8. DOI: [10.1109/HPEC49654.2021.9622805](https://doi.org/10.1109/HPEC49654.2021.9622805).
- [48] Shaoyi Huang et al. “Neurogenesis Dynamics-inspired Spiking Neural Network Training Acceleration.” *2023 60th ACM/IEEE Design Automation Conference (DAC)*. 2023 60th ACM/IEEE Design Automation Conference (DAC). 2023, pp. 1–6. DOI: [10.1109/DAC56929.2023.10247810](https://doi.org/10.1109/DAC56929.2023.10247810).
- [49] Elvin Hajizada et al. *Real-time Continual Learning on Intel Loihi 2*. 2025. DOI: [10.48550/ARXIV.2511.01553](https://doi.org/10.48550/ARXIV.2511.01553).
- [50] Marcel Stimberg, Romain Brette, and Dan F.M. Goodman. “Brian 2, an intuitive and efficient neural simulator.” *eLife* 8 (2019), pp. 1–41. DOI: [10.7554/eLife.47314](https://doi.org/10.7554/eLife.47314).
- [51] Charl Linssen et al. “NESTML: a generic modeling language and code generation tool for the simulation of spiking neural networks with advanced plasticity rules.” *Frontiers in Neuroinformatics* 19 (2025), p. 1544143. DOI: [10.3389/fninf.2025.1544143](https://doi.org/10.3389/fninf.2025.1544143).
- [52] Levin Schmidt. “Extension of the NEST Modelling Language to the SpiNNaker Architecture.” PhD thesis. Aachen: RWTH Aachen University, 2023.
- [53] Hector A. Gonzalez et al. *SpiNNaker2: A Large-Scale Neuromorphic System for Event-Based and Asynchronous Machine Learning*. 2024. arXiv: [2401.04491](https://arxiv.org/abs/2401.04491)[cs].
- [54] Mike Davies et al. “Loihi : a Neuromorphic Manycore Processor with On-Chip Learning.” *IEEE Micro* 30.1 (2018), pp. 82–99. DOI: [10.1109/MM.2018.112130359](https://doi.org/10.1109/MM.2018.112130359).